



Micro-article

Computer-assisted pre-operative automatic segmentation and registration tool for malunited radius osteotomy: A proof-of-concept study

Jiaqiu Wang^{a,b,*}, Robert Zietal^c, Alexander Arase^a, Greg Couzens^{a,d}, Peter Pivonka^{a,b}, Davide Fontanarosa^{b,c,*}

^a School of Mechanical, Medical and Process Engineering, Queensland University of Technology, Brisbane, 4000, QLD, Australia

^b Centre for Biomedical Technologies, Queensland University of Technology, Brisbane, 4000, QLD, Australia

^c School of Clinical Sciences, Queensland University of Technology, Brisbane, 4000, QLD, Australia

^d Brisbane Hand & Upper Limb Clinic, Brisbane, 4000, QLD, Australia

ARTICLE INFO

Keywords:

Malunited radius
Corrective osteotomy
Pre-operative plan

ABSTRACT

Corrective osteotomy is a standard treatment for distal radius fractures in malunited radius cases. In order to increase the efficiency of the osteotomy pre-operative plan, in this study, a proof-of-concept framework of automatic computer-assisted segmentation and registration tool was developed for the purpose of malunited radius osteotomy pre-operative planning. The program consisted of the functions of segmentation, virtual cutting, automatic alignment and registration. One computed tomography (CT) scanning dataset of a patient's bilateral forearm was employed as an illustration example in this study. Three templates of 3D models including the healthy radius, and the pre- and post-correction injured radius were output as STL geometries for pre-operative plan purposes.

1. Introduction

Distal radius fracture is a common injury [1][2], for which malunion is one of the most commonly reported complications [3][4][5]. It may lead to dorsal tilt and radial length shortening, which could cause radiocarpal and radioulnar pain, and limitations in forearm supination and pronation [6][7][8].

For the treatment of this complication, the corrective osteotomy is a standard treatment used in clinical practice [9][10]. The main objective of corrective osteotomy is to restore the injured radius to the pre-injury anatomical form. Using radiographic imaging with anteroposterior, lateral, and oblique views, the deformity is defined by the appropriate ulnar variance, radial height, radial inclination, and volar tilt. Based on these parameters, the injured radius is cut around the fracture location, and the injured segment is aligned to its pre-injury anatomical position. The wedged gap between the segments of the injured radius is connected with an osteosynthesis plate, which was stabilized using screws fixed on both segments [11][12][13]. However, the conventional corrective osteotomy still has challenges due to the complex deformity of the bone geometry [14][15]. For example, from 2D planar imag-

ing data, it is only possible to measure the displacement and rotation with three degrees of freedom (DOF), while from 3D imaging data, the measurement of the displacement and rotation have six DOF, which provides more precise parameter evaluation, such as rotational deformity, that commonly occurs with angulated malunions of distal radius [16][17][18]. Comparatively, a more advanced 3D model-based corrective osteotomy typically uses three radius templates, i.e. the radius models of both forearms (healthy side and injured side), and the corrective injured radius. The healthy and injured radii are reconstructed from radiographic imaging data. The deformity of the injured radius is evaluated by superimposing it onto the mirrored healthy radius model. Then a virtual cut divides the injured radius at the malunion location into proximal and distal sections. These two sections are re-aligned based on the mirrored healthy radius model again. Finally, the realigned injured radius (both proximal and distal sections) is output as the corrective radius model, which is used as a reference to the real surgery. This technology brings the surgeon clear visualization of the malunions, and helps the surgeon with the patient-specific osteotomy plan including surgical cut and the plate fixation [19][20], it provides high accuracy of the osteotomy plan [21], and in the meantime, improve the pre-operative plan efficiency [22].

* Corresponding authors.

E-mail addresses: jiaqiu.wang@qut.edu.au (J. Wang), d3.fontanarosa@qut.edu.au (D. Fontanarosa).

<https://doi.org/10.1016/j.rineng.2023.101295>

Received 15 March 2023; Received in revised form 5 July 2023; Accepted 11 July 2023

Available online 26 July 2023

2590-1230/© 2023 The Author(s). Published by Elsevier B.V. This is an open access article under the CC BY license (<http://creativecommons.org/licenses/by/4.0/>).

The complexity of the 3D radius structure requires a precise pre-operation plan to guarantee the quality of corrective osteotomy [23]. To improve the conventional corrective osteotomy, computer-assisted osteotomy plan technology has been rapidly developing and is able to help on each substep of the pre-operation plan, including computed tomography (CT) imaging processing, bone structure segmentation and reconstruction, corrective registration, patient-specific plate design, etc [24][25][26]. In detail, CT imaging data typically show sharp boundaries between cortical bone and surrounding soft tissue and is used as the gold standard for 3D modelling of bone structure [27] and medical device manufacturing [28]. Several algorithms, such as grey level thresholding masks, contour estimation/correction algorithm, and watershed method have been introduced in the segmentation of bone structures from CT scans [29][30][31]. By virtue of anatomical chirality of the radii of the injured and healthy sides, the healthy structure of the injured side could be assumed by computational registering with the healthy side radius [32][33]. From the registered models, the cut plane, angle, and position for the injured radius osteotomy could be estimated. With computational modelling, the malunited part correction, the osteosynthesis plate, and jigs position could be visualized and evaluated [34][22]. The computer-assisted biomechanical analysis could help with the design of customised-healthcare products such as corrective plate, implant, and scaffold, by 3D printing prototype [35][36][37][38] and finite element analysis (FEA) [39][40].

By integrating the aforementioned methods, algorithms, and technologies, some computer-assisted osteotomy pre-operative plan protocols and tools have been reported. Schweizer et al. [41] reported a computer-assisted osteotomy planning workflow, including the imaging acquisition, 3D reconstruction, registration, and alignment steps. The key idea was using a 3D model to perform interactively virtual cut and repositioning. The iterative closest point (ICP) automatic registration method [42] was employed. In the end, the required parameters of rotation and translation could be exported from the obtained transformation matrices. Carrillo et al. [22] proposed an automatic multi-objective 3D pre-operative plan method. Besides the objectives of evaluating the alignment and cut plane, the proposed method also included the objectives of optimizing the plate allocation and screw fixation. Their clinical validation proved that the proposed computer-assisted osteotomy plan was an accurate and time-saving approach. Dobbe et al. [43][18][44] published a series study about their custom-made pre-operative plan software, which included the functions of finding the repositioning parameters, cutting guide, and patient-tailored plate. This custom-made software was further extended as a semi-automatic design tool for 3D-printed patient-specific instruments (PSIs) [45].

The current pre-operative osteotomy plan methods do not come without their own challenges. Several limitations are still present, for example, self-adaptive parameters setup among different objectives, reducing the human interactive workloads, and improving the process efficiency [22][45]. In order to increase the efficiency of the procedure, an automatic algorithm with a friendly user interface (UI) was developed in MATLAB (The MathWorks, Inc., Natick, Massachusetts, USA) in this proof-of-concept study. A self-adapting threshold-based segmentation process was designed to reconstruct both injured and healthy sides on a bilateral high-resolution forearm CT scan. The injured radius was then fused onto the mirrored, healthy one. The injured radius was 'cut' into proximal and distal subsections and were repositioned based on the corresponding structure in the healthy radius. All the geometries produced were then output as STL files for osteotomy pre-operative plan purposes.

2. Materials and methods

A bilateral forearm CT scan (TOSHIBA Aquilion ONE) was employed to develop and verify the algorithm. The CT scan protocol Sugicase CT Forearm was used for imaging acquisition. The acquisition resolution of each CT imaging slice was 512×512 . In total 1381 slices were ac-

quired in the CT imaging sequence. The CT scanning data was stored following the DICOM transfer protocol and all the sensitive data were anonymized.

The proposed algorithm was developed in MATLAB with an object-oriented design. The main concept was to automatically segment, register and reconfigure the injured bone comparing it to the healthy one after chirality has been removed through mirroring. A flow chart of the program design is shown in Fig. 1. The algorithm was developed to have functional modules including: pre-processing, segmentation, mirror transformation, visualization, registration, and corrective configuration.

Pre-processing was required to sort up the input dataset and to initialize the parameters required for the program. The imported DICOM sequence was converted to a volumetric matrix in MATLAB for the subsequent processes. Also, the forearms of the injured and healthy sides were labelled. For the purpose of removing the chirality of the healthy and injured sides, a mirrored dataset was created from the CT scan, so that the injured arm could be registered on the mirrored healthy geometry. A friendly user interface (UI) was designed for the algorithm in MATLAB to manage the data input, initialization, and visualization tasks.

2.1. Segmentation

Segmentation was the first major functional module in this algorithm, which outlined the bone structure from the other tissues.

The first step in the segmentation process was to generate the CT volumetric matrix and standardize the intensity into a uniform intensity range [0,1]. Then the region of interest (ROI) was defined to isolate the bone area and to block out the part which had a similar intensity range as the bone structure.

The processed volumetric matrix was then binarized to present the bone structure only. In the binarized data, there were still some hollow areas within the bone boundary, which would be filled and generated the final bone mask. Subsequently, the binarized matrix was transformed and represented as a $n \times 3$ array, where n was the total number of voxels with bone, and each voxel consisted of three spatial coordinate components. The final step was to transform the voxel representation into a triangulated object. This was achieved by converting the voxels representation into an alpha shape (with an alpha radius of 1). The surface of bone geometry was then described by using boundary facets, which could be output as standard STL files. The visualization module would also provide an in-built view of the segmented bone as an STL file.

To verify the developed automatic segmentation method, a comparison was performed with manual segmentation of the radius performed by an experienced orthopedic surgeon, using ITK-snap [46]. The Sørensen–Dice similarity coefficient (DSC) method was used as a metric to evaluate the segmentation quality.

2.2. Registration

After segmentation, the healthy radius was mirrored through coordinates transformation to remove the chirality between the two radii, and then overlaid onto the injured radius. The two radii were virtually cut into proximal (to the patient's body) and distal subsections. The length ratio of the two subsections was pre-determined by clinicians based on patient cases. An initial alignment was performed based on the proximal subsection since it was the one not affected by the injury in the malunited radius. The radius geometries were transformed from voxelised data into a point cloud dataset for registration. The registration was performed by superimposing the mirrored, healthy radius onto the injured one by using the point-cloud transform function in Matlab. The root mean square (RMS) was used to measure these two geometries with the minimum gap between them.

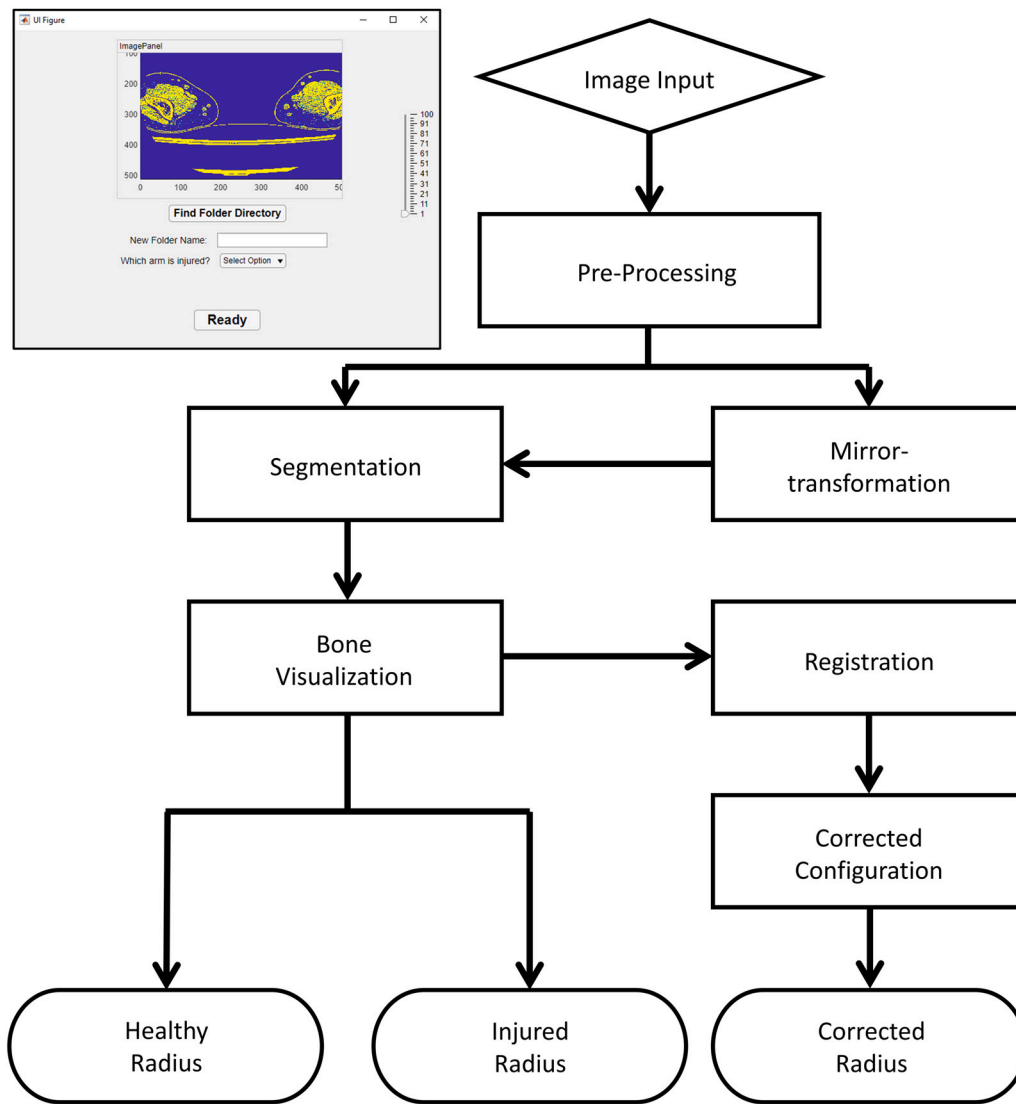


Fig. 1. The flow chart of the algorithm design. The imaging data were firstly pre-processed and mirrored, which provided the healthy geometry with chirality removed. The bone structure of mirrored healthy side and injured side were then segmented. The injured bone was corrected by registering it onto the healthy geometry provided by the mirrored healthy side bone structure. To achieve this, the designed functional modules included: pre-processing, segmentation, mirror transformation, visualization, registration, and corrective configuration. The top left corner is the user interface (UI) of the proposed program which was developed in Matlab. The start-up UI page allows users to select the working folder directory, output the folder name, and define the injured side. It also provides a preview window where CT imaging samples from the input sequence could be previewed. A sliding bar allows the user to select the slices to preview easily.

2.3. Corrective configuration

To obtain the final corrective position, besides the proximal alignment described in the previous section, the distal subsections needed to be re-aligned and registered onto the corrective position. To achieve it, the registration used the whole mirrored, healthy radius, which was firstly transformed onto the injured radius position by applying the same transformation matrix calculated from the previous proximal registration. The distal portion on this healthy radius geometry was treated as an accurate template for the registration of the injured distal subsection. The distal subsection of the injured radius was then registered onto the distal portion of the healthy radius.

As output, the radius geometry of the injured radius, the healthy radius (mirrored), and the pre-operative plan view, which was generated by re-aligning the injured subsections based on the healthy radius, were exported as STL geometric files.

3. Results

Fig. 2 presents the imaging slices from four locations from proximal to distal. By means of high-resolution CT imaging, the bone structure could be clearly visualized from the original CT dataset. During the processing, the ROI was cropped to reduce the redundant area (mainly the top and bottom areas in the image). After adjusting the pixel intensity, the bone structure was given prominence from the background. The binarization thresholding boundaries used here were 97.5% of the standardized intensity value. From the binarized CT data, the boundary of the bone structure was clearly segmented, which generated the surface of the bone structure in 3D. Noticing that the binarization only still could not provide the perfect bone model yet, there was still some noise and the inconsistent hollow area within the bone surface. It required a subsequent process to remove the isolated noise using area size filtering, and to generate a bone mask to fill the whole volume within the bone surfaces.

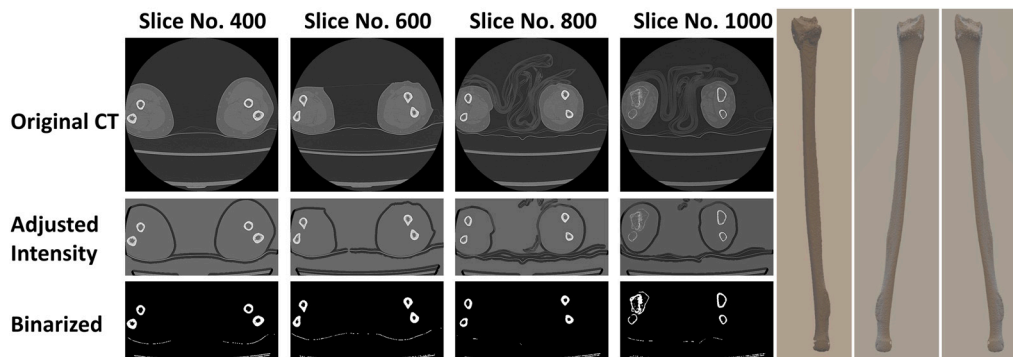


Fig. 2. The 2D slice samples of original CT imaging data, intensity-adjusted data, and binarized data at the slice number of 400, 600, 800, and 1000. Note that the region of interest (ROI) of intensity-adjusted data and binarized data were already cropped during the process. And in the binarized imaging data, there were still some discrete noises, which were further removed by using area filter. The right hand side is the reconstructed radius STLs. From left to right are injured, healthy and mirrored healthy structures, respectively.

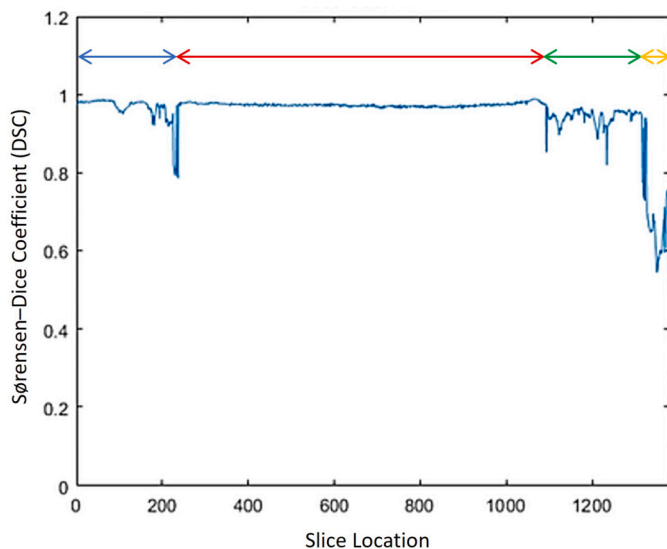


Fig. 3. The segmentation results were verified by using benchmark results which were manually segmented by an experienced orthopedic surgeon. The Sørensen–Dice coefficient (DSC) from the comparison results of the program and manual segmentation on each CT scan slice was used as the index of the verification. For most of the results, the coefficients were above 0.95 (red arrow indicated region). The two drops at around the 200th (blue arrow) and the 1100th (green arrow) slices were because of the articulation joint. The values after the 1250th slice (yellow arrow) could be neglected as the corresponding region was outside the region of interest.

The Sørensen–Dice similarity coefficient (DSC) metric between the segmentation results from the proposed algorithm and the benchmark from an experienced clinician are shown slice by slice in Fig. 3. For most of the slices (from slice 300 to slice 1000) the accuracy was close to 1. Around slice number 200, there was a significant drop in the DSC caused by the articulation joint between the ulnar-radius and humerus. Another similar drop occurs around slice number 1100 at the intersection between the radius and the carpal bones. For most of the slices at these joint locations, the accuracy was around 0.95. In the slices above 1250, the metacarpus was imaged, which was not part of the region of interest for this work and, as such, could be neglected.

Fig. 4(A&B) presents a visualisation of the radius registration. The radius structures in the registration process were presented using the cloud point format. The mirrored, healthy radius (green), and injured radius (red) were used in the registration. The registration process had two sub-steps. Firstly, both radii were divided into proximal and distal subsections. In this case, the division was based on the length ratio of 85% and 15%. As the proximal subsection of the injured radius was

not affected by the injury, the proximal subsection of the healthy radius could be perfectly registered to the proximal subsection of the injured side first. Then in the next sub-step, the whole healthy radius was transferred using the same transfer matrix from the last sub-step. Finally, based on the shape and location of the distal portion of the transferred mirrored healthy radius, the distal subsection of the injured radius was registered to the corrective position. Fig. 4(C&D) shows the enlarged cloud point view of the registration of distal subsections. The registration and the subsequent corrective configuration of the injured radius were visually evaluated by an experienced orthopedic surgeon.

The algorithm output three geometric files in STL format for surgery reference, including the mirrored healthy radius, which was used as the reference of corrective radius geometry; the injured radius, which could be used for verifying the segmentation and reconstruction with original CT imaging data; and the corrective position of the subsections of injured radius, which could be used as a reference for the surgical plan (Fig. 5).

4. Discussion

This study proposed a framework of a computer-assisted osteotomy pre-operative plan tool for malunited radius. The concept of this algorithm design considered the chirality of the left and right arms and used the geometry from the healthy side as a benchmark to correct the radius geometry of the injured side. This tool aimed to provide intuitionistic visualisation of the 3D models of the patient’s radius to clinicians to assist the pre-operative plan. The comparison of the radius from both the injured and healthy sides clearly showed the patient’s injury conditions. The provided corrective structure from this proposed tool would be a great help to virtually planning the operation. The models could also be 3D-printed for designing the treatment plan and mimicking the operative process.

Compared to other semi-automatic approaches, which required user interactions during the process, the proposed program only required some key parameters such as dataset selection, binarization thresholding, and cutting position to be pre-described before the program ran. After the program began the process, all steps of imaging processing, segmentation, and registration ran automatically without the manual interaction required. For process efficiency, the current version of the algorithm ran around one hour on a computer with 16 GB RAM, Intel® Core i7 CPU (2.80 GHz).

At the current stage, the designed framework had integrated the imaging-processing modules, mainly including the algorithms and functions of segmentation, registration and corrective configuration. Besides the radius, the proposed framework could be adaptive to be used for other fracture problems such as the ulnar shortening and malalignment [47][48]. The concept of the algorithm required the patient has both arms scanned. And it was assumed that the bones in both arms had

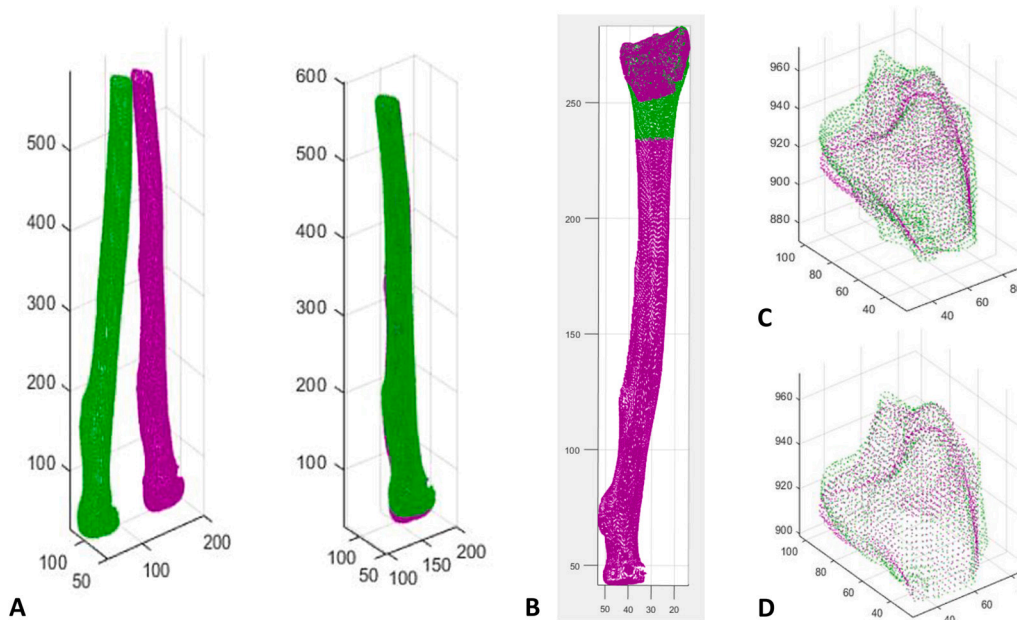


Fig. 4. Example of the registration process. The radii were presented as cloud points here, the green one was mirrored, healthy radius and the red one was the injured radius. The registration process was divided into two sub-steps: A) the proximal subsection of mirrored, healthy radius was firstly registered to the proximal subsection of the injured side; B) then the whole mirrored healthy radius was transferred using the same transfer matrix. Finally, based on the shape and location of the distal portion of the transferred mirrored healthy radius, the distal subsection of the injured radius was registered to the corrective position. The corrective configuration was visually evaluated by an experienced orthopedic surgeon. Subplots C&D provide the enlarged view of the registration of the distal (injured) subsection. The distal subsections were presented as cloud points here, the green one was mirrored, healthy radius and the red one was the injured radius: C) pre-registration; D) post-registration, the injured distal subsection and the counterpart at mirrored, healthy geometry were well-aligned. The registration result of the injured radius was visually evaluated by an experienced orthopedic surgeon.

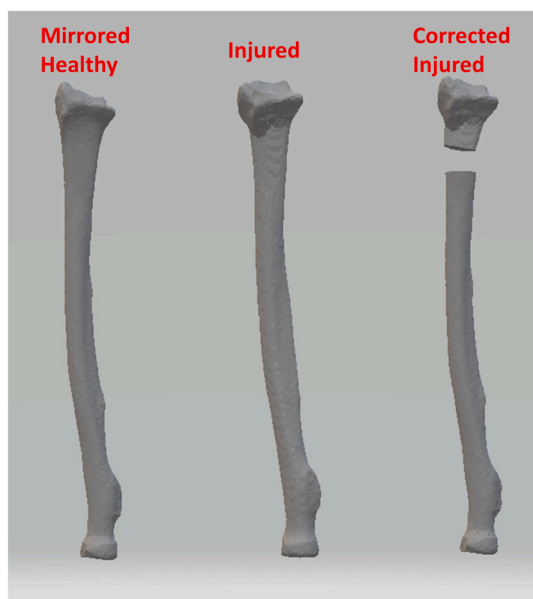


Fig. 5. Examples of output radius geometries as STL files. From left to right, the mirrored healthy radius; the injured radius; the corrected sample of the injured radius after registration with the mirror healthy radius.

very similar structures. Previous studies showed evidence of the variance between bilateral bone geometries, which may cause bias in the correction osteotomy based on the contralateral healthy radius as a reference. However, in most real clinical cases, the geometric data of the original radius before the injury is unknown and no better reference is available for the osteotomy plan, so the mirrored healthy side is usually considered as a reasonable reference [32][49]. Besides, in some scenarios, (for example, if the imaging data does not include both fore-

arms, or the bone was injured on both sides), the algorithm may also not work properly. The robustness of the algorithm and the tolerance of the bilateral side variance will be further investigated in future studies. Another determinant for guaranteeing the quality of segmentation, reconstruction and registration of bone geometry would be the CT imaging quality. If the imaging quality was affected by the artefacts such as metal implants, the voxel intensity of CT imaging data might have large variation, because metals' density is larger than bones', which might cause large amounts of artefact and noise [50][51].

As a proof-of-the-concept study, which aimed to provide an overview of the framework design of the proposed tool, one of the limitations of this study is that only one dataset was included to show the procedure of the imaging processing tasks. Before the tool can be translated to clinical trial, the robustness of the developed tool requires to be optimised and verified by conducting large group patient data study. Besides the current used validating measurements, more clinical-meaningful creation will be requested to justify the precision of segmentation and registration. Another improvement direction will be to promote the automation level of the algorithm to be compatible with wide-range patient-specific cases. For example, the determination parameters of the binarization threshold, and proximal/distal subsections in the current algorithm were pre-described by using the values suggested by clinicians, which highly relied on clinicians' experience and skills. In future development, these setup parameters will be optimised to be automatically or semi-automatically configured based on large-scope patient case training. Also, the current algorithm lacked the necessary instructions and warnings to provide to the end-users, this function is also listed in the future translated study. To further accelerate the process, the potential optimisation for future development will be simplifying the dataset structure or transplanting the algorithm into a more efficient code environment. For the future clinical use version, the algorithm will be expected to process the data at least four times faster than the current version.

Before it can be finally used in clinical practice, this algorithm still misses some key functions and features, which have been planned for the future. Although the current output 3D geometries have provided clinicians with a direct preview of healthy, injured and corrective radii, the key quantitative parameters used in operation, such as gap created from the correction, angle of the articulating surface, rotation of the distal section are not yet provided as the surgical guide. Another main function of the osteotomy pre-operative plan tool is the plate design and its fixation. The current stage of study mainly focused on the imaging processing module, therefore, has not included the function of planning the plate-screw system. In the next-step development plan, to provide the customized design of the plate and its fixation in surgery, a patient-specific plate design module will be developed based on the output of the introduced imaging processing module. As the biomechanical stress has been proven to have a strong relationship with the plate-screw system [52][53][54], the plate-screw fixation in the surgery is required to be further investigated through the biomechanical analysis based on finite element method (FEM) simulation. The relevant feature of implanted plates design and screw fixture positions will be designed and added to the current development of the algorithm. In the final commercialised surgery-assist software, a comprehensive report will be provided to clinicians, which includes all the necessary information about the patient-specific reconstructed healthy and injured bone geometry, the pre-operative plan for treating injured bone, and the simulated post-surgery effect.

5. Conclusion

Overall, this proof-of-the-concept study developed a computer-assisted pre-operative automatic segmentation and registration tool for the purpose of an osteotomy pre-operative plan. The concept and current framework have shown great potential to be used to assist clinicians in surgical plans. More extensive group patient data study, algorithm optimization and new functional features development are required in the future development to fill the gap of its final translation to clinical practice.

Ethical approval

The Queensland University of Technology Human Research Ethics Committee confirmed that this research is exempt from human research ethics review in accordance with the National Statement on Ethical Conduct in Human Research (2007, updated 2018).

Declaration of competing interest

The authors declare that they have no known competing financial interests or personal relationships that could have appeared to influence the work reported in this paper.

Data availability

The data that has been used is confidential.

Funding

The authors would like to acknowledge the financial support from the Early Career Researcher Grant funded by Centre for Biomedical Technologies, Queensland University of Technology (QUT).

References

- [1] K.C. Chung, S.V. Spilson, The frequency and epidemiology of hand and forearm fractures in the United States, *J. Hand Surg.* 26 (2001) 908–915, <https://doi.org/10.1053/jhsu.2001.26322>.
- [2] D.A. London, R.P. Calfee, 60 - distal radius fractures, in: G.E. Garrigues, M.J. Richard, M.J. Gage (Eds.), *Skeletal Trauma of the Upper Extremity*, Elsevier, Philadelphia, 2022, pp. 470–484.
- [3] B.D. Bushnell, D.K. Bynum, Malunion of the distal radius, *J. Am. Acad. Orthop. Surg.* 15 (2007) 27–40, <https://doi.org/10.5435/00124635-200701000-00004>.
- [4] F.A. Liporace, M.R. Adams, J.T. Capo, K.J. Koval, Distal radius fractures, *J. Orthop. Trauma* 23 (2009) 739–748, <https://doi.org/10.1097/BOT.0b013e3181ba46d3>.
- [5] K.-J. Prommersberger, T. Pillukat, M. Mühlendorfer, J. van Schoonhoven, Malunion of the distal radius, *Arch. Orthop. Trauma Surg.* 132 (2012) 693–702, <https://doi.org/10.1007/s00402-012-1466-y>.
- [6] R.J. Butler, S. Marchesi, T. Royer, I.S. Davis, The effect of a subject-specific amount of lateral wedge on knee mechanics in patients with medial knee osteoarthritis, *J. Orthop. Res.* 25 (2007) 1121–1127, <https://doi.org/10.1002/jor.20423>.
- [7] J.-M. Cognet, O. Mares, Distal radius malunion in adults, *Orthop. Traumatol., Surg. Res.* 107 (2021) 102755, <https://doi.org/10.1016/j.otsr.2020.102755>.
- [8] P.H. Stirling, W.M. Oliver, N. Ng, C.W. Oliver, M.M. McQueen, S.G. Molyneux, A.D. Duckworth, Distal radius malunion: outcomes following an ulnar shortening osteotomy, *Eur. J. Orthop. Surg. Traumatol.* (2022) 1–6, <https://doi.org/10.1007/s00590-022-03325-9>.
- [9] D. Paley, *Principles of Deformity Correction*, Springer Science & Business Media, 2002.
- [10] M.W. Patton, Distal radius malunion, *J. Am. Soc. Surg. Hand* 4 (2004) 266–274, <https://doi.org/10.1016/j.jassh.2004.09.007>.
- [11] K. Prommersberger, J. Van Schoonhoven, U. Lanz, Outcome after corrective osteotomy for malunited fractures of the distal end of the radius, *J. Hand Surg. (British & European)* 27 (2002) 55–60, <https://doi.org/10.1054/jhsb.2001.0693>.
- [12] M. Brown, K.C. Chung, Procedure 32 - corrective osteotomy of radius malunion, in: K.C. Chung (Ed.), *Operative Techniques: Hand and Wrist Surgery, third edition*, Elsevier, 2018, pp. 312–325.
- [13] G. Caiti, J.G. Dobbe, S.D. Strackee, G.J. Srijkers, G.J. Streekstra, Computer-assisted techniques in corrective distal radius osteotomy procedures, *IEEE Rev. Biomed. Eng.* 13 (2019) 233–247, <https://doi.org/10.1109/RBME.2019.2928424>.
- [14] S. Lozano-Calderon, K. Brouwer, J. Doornberg, J. Carel Goslings, P. Kloen, J. Jupiter, Long-term outcomes of corrective osteotomy for the treatment of distal radius malunion, *J. Hand Surg. (Eur. Vol.)* 35 (2010) 370–380, <https://doi.org/10.1177/1753193409357373>.
- [15] B. Katt, D. Seigerman, K. Lutsky, P. Beredjikian, Distal radius malunion, *J. Hand Surg.* 45 (2020) 433–442, <https://doi.org/10.1016/j.jhsa.2020.02.008>.
- [16] K.-J. Prommersberger, S.C. Froehner, R.R. Schmitt, U.B. Lanz, Rotational deformity in malunited fractures of the distal radius, *J. Hand Surg.* 29 (2004) 110–115, <https://doi.org/10.1016/j.jhsa.2003.09.014>.
- [17] J.G. Dobbe, K. Du Pré, P. Kloen, L. Blankevoort, G.J. Streekstra, Computer-assisted and patient-specific 3-d planning and evaluation of a single-cut rotational osteotomy for complex long-bone deformities, *Med. Biol. Eng. Comput.* 49 (2011) 1363–1370, <https://doi.org/10.1007/s11517-011-0830-3>.
- [18] J.G. Dobbe, J.C. Vroemen, S.D. Strackee, G.J. Streekstra, Patient-tailored plate for bone fixation and accurate 3d positioning in corrective osteotomy, *Med. Biol. Eng. Comput.* 51 (2013) 19–27, <https://doi.org/10.1007/s11517-012-0959-8>.
- [19] R. de Muinck Keizer, K. Lechner, M. Mulders, N. Schep, D. Eygendaal, J. Goslings, Three-dimensional virtual planning of corrective osteotomies of distal radius malunions: a systematic review and meta-analysis, *Strat. Trauma Limb Reconstr.* 12 (2017) 77–89, <https://doi.org/10.1007/s11751-017-0284-8>.
- [20] M. Walenkamp, R. de Muinck Keizer, J. Dobbe, G. Streekstra, J. Goslings, P. Kloen, S. Strackee, N. Schep, Computer-assisted 3d planned corrective osteotomies in eight malunited radius fractures, *Strat. Trauma Limb Reconstr.* 10 (2015) 109–116, <https://doi.org/10.1007/s11751-015-0234-2>.
- [21] F. Stockmans, M. Dezillie, J. Vanhaecke, Accuracy of 3d virtual planning of corrective osteotomies of the distal radius, *J. Wrist Surg.* 2 (2013) 306–314, <https://doi.org/10.1055/s-0033-1359307>.
- [22] F. Carrillo, L. Vlachopoulos, A. Schweizer, L. Nagy, J. Snedeker, P. Fürnstahl, A time saver: optimization approach for the fully automatic 3d planning of forearm osteotomies, in: *International Conference on Medical Image Computing and Computer-Assisted Intervention*, Springer, 2017, pp. 488–496.
- [23] J.C. Belloti, B.V.P. Alves, F. Faloppa, D. Balbachevsky, N.A. Netto, M.J. Tamaoki, The malunion of distal radius fracture: corrective osteotomy through planning with prototyping in 3d printing, *Injury* 52 (2021) S44–S48, <https://doi.org/10.1016/j.injury.2021.05.048>.
- [24] G.S. Athwal, R.E. Ellis, C.F. Small, D.R. Pichora, Computer-assisted distal radius osteotomy, *J. Hand Surg.* 28 (2003) 951–958, [https://doi.org/10.1016/S0363-5023\(03\)00375-7](https://doi.org/10.1016/S0363-5023(03)00375-7).
- [25] J. Schneppendahl, J. Windolf, R.A. Kaufmann, Distal radius fractures: current concepts, *J. Hand Surg.* 37 (2012) 1718–1725, <https://doi.org/10.1016/j.jhsa.2012.06.001>.
- [26] G. Caiti, J.G. Dobbe, E. Bervoets, M. Beerens, S.D. Strackee, G.J. Srijkers, G.J. Streekstra, Biomechanical considerations in the design of patient-specific fixation plates for the distal radius, *Med. Biol. Eng. Comput.* 57 (2019) 1099–1107, <https://doi.org/10.1007/s11517-018-1945-6>.
- [27] K. Rathnayaka, T. Sahama, M.A. Schuetz, B. Schmutz, Effects of ct image segmentation methods on the accuracy of long bone 3d reconstructions, *Med. Eng. Phys.* 33 (2011) 226–233, <https://doi.org/10.1016/j.medengphy.2010.10.002>.
- [28] M. Van Eijnatten, R. van Dijk, J. Dobbe, G. Streekstra, J. Koivisto, J. Wolff, Ct image segmentation methods for bone used in medical additive manufacturing, *Med. Eng. Phys.* 51 (2018) 6–16, <https://doi.org/10.1016/j.medengphy.2017.10.008>.

- [29] L. Vincent, P. Soille, Watersheds in digital spaces: an efficient algorithm based on immersion simulations, *IEEE Trans. Pattern Anal. Mach. Intell.* 13 (1991) 583–598, <https://doi.org/10.1109/34.87344>.
- [30] W. Yao, P. Abolmaesumi, M. Greenspan, R.E. Ellis, An estimation/correction algorithm for detecting bone edges in ct images, *IEEE Trans. Med. Imaging* 24 (2005) 997–1010, <https://doi.org/10.1109/TMI.2005.850541>.
- [31] S. Vasilache, K. Najarian, Automated bone segmentation from pelvic ct images, in: *2008 IEEE International Conference on Bioinformatics and Biomedicine Workshops, IEEE, 2008*, pp. 41–47.
- [32] J. Vroemen, J. Dobbe, R. Jonges, S. Strackee, G. Streekstra, Three-dimensional assessment of bilateral symmetry of the radius and ulna for planning corrective surgeries, *J. Hand Surg.* 37 (2012) 982–988, <https://doi.org/10.1016/j.jhsa.2011.12.035>.
- [33] F. Mauler, C. Langguth, A. Schweizer, L. Vlachopoulos, T. Gass, M. Lüthi, P. Fürnstahl, Prediction of normal bone anatomy for the planning of corrective osteotomies of malunited forearm bones using a three-dimensional statistical shape model, *J. Orthop. Res.* 35 (2017) 2630–2636, <https://doi.org/10.1002/jor.23576>.
- [34] M. Kunz, B. Ma, J.F. Rudan, R.E. Ellis, D.R. Pichora, Image-guided distal radius osteotomy using patient-specific instrument guides, *J. Hand Surg.* 38 (2013) 1618–1624, <https://doi.org/10.1016/j.jhsa.2013.05.018>.
- [35] T. Tom, S.P. Sreenilayam, D. Brabazon, J.P. Jose, B. Joseph, K. Madanan, S. Thomas, Additive manufacturing in the biomedical field-recent research developments, *Results Eng.* (2022) 100661, <https://doi.org/10.1016/j.rineng.2022.100661>.
- [36] A. Bafor, J. Parthasarathy, C.A. Jobst, 3d printing in pediatric orthopedics, *Bone Tissue Eng.* (2022) 149–164, https://doi.org/10.1007/978-3-030-92014-2_7.
- [37] C.J.A. Mendonça, J.A.P. Setti, 3d printing in orthopedic surgery, in: *Personalized Orthopedics*, Springer, 2022, pp. 375–409.
- [38] T. Daoulas, H. Letissier, F. Dubrana, R. Di Francia, Corrective osteotomy of a distal radius malunion using three-dimensional custom guides, in: *Annals of 3D Printed Medicine*, 2023, 100099.
- [39] A. Synek, S.F. Baumbach, D.H. Pahr, Towards optimization of volar plate fixations of distal radius fractures: using finite element analyses to reduce the number of screws, *Clin. Biomech.* 82 (2021) 105272, <https://doi.org/10.1016/j.clinbiomech.2021.105272>.
- [40] L. Wang, J. Wang, Q. Chen, Q. Li, J.B. Mendieta, Z. Li, How getting twisted in scaffold design can promote bone regeneration: a fluid–structure interaction evaluation, *J. Biomech.* 145 (2022) 111359, <https://doi.org/10.1016/j.jbiomech.2022.111359>.
- [41] A. Schweizer, P. Fürnstahl, M. Harders, G. Székely, L. Nagy, Complex radius shaft malunion: osteotomy with computer-assisted planning, *Hand* 5 (2010) 171–178, <https://doi.org/10.1007/s11552-009-9233-4>.
- [42] Y. Chen, G. Medioni, Object modelling by registration of multiple range images, *Image Vis. Comput.* 10 (1992) 145–155, [https://doi.org/10.1016/0262-8856\(92\)90066-C](https://doi.org/10.1016/0262-8856(92)90066-C).
- [43] J.G. Dobbe, S.D. Strackee, A. Schreurs, R. Jonges, B. Carelsen, J.C. Vroemen, C.A. Grimbergen, G.J. Streekstra, Computer-assisted planning and navigation for corrective distal radius osteotomy, based on pre-and intraoperative imaging, *IEEE Trans. Biomed. Eng.* 58 (2010) 182–190, <https://doi.org/10.1109/TBME.2010.2084576>.
- [44] J.G. Dobbe, S.D. Strackee, G.J. Streekstra, Minimizing the translation error in the application of an oblique single-cut rotation osteotomy: where to cut?, *IEEE Trans. Biomed. Eng.* 65 (2017) 821–827, <https://doi.org/10.1109/TBME.2017.2721498>.
- [45] G. Caiti, J.G. Dobbe, A.C. Loenen, M. Beerens, S.D. Strackee, G.J. Strijkers, G.J. Streekstra, Implementation of a semiautomatic method to design patient-specific instruments for corrective osteotomy of the radius, *Int. J. Comput. Assisted Radiol. Surg.* 14 (2019) 829–840, <https://doi.org/10.1007/s11548-018-1896-2>.
- [46] P.A. Yushkevich, J. Piven, H. Cody Hazlett, R. Gimpel Smith, S. Ho, J.C. Gee, G. Gerig, User-guided 3D active contour segmentation of anatomical structures: significantly improved efficiency and reliability, *NeuroImage* 31 (2006) 1116–1128, <https://doi.org/10.1016/j.neuroimage.2006.01.015>.
- [47] K. Barbaric, G. Rujevcan, M. Labas, D. Delimar, G. Bicanic, Ulnar shortening osteotomy after distal radius fracture malunion: review of literature, *Open Orthop. J.* 9 (2015) 98, <https://doi.org/10.2174/1874325001509010098>.
- [48] M.C. Tynan, S. Fornalski, P.J. McMahon, A. Utkan, S.A. Gree, T.Q. Lee, The effects of ulnar axial malalignment on supination and pronation, *J. Bone Jt. Surg.* 82 (2000) 1726, <https://doi.org/10.2106/00004623-200012000-00005>.
- [49] N. Hollevoet, R. Verdonk, The functional importance of malunion in distal radius fractures, *Acta Orthop. Belg.* 69 (2003) 239–245.
- [50] T.M. Coupal, P.I. Mallinson, P. McLaughlin, S. Nicolaou, P.L. Munk, H. Ouellette, Peering through the glare: using dual-energy ct to overcome the problem of metal artefacts in bone radiology, *Skelet. Radiol.* 43 (2014) 567–575, <https://doi.org/10.1007/s00256-013-1802-5>.
- [51] S. Kohyama, Y. Yoshii, Y. Okamoto, T. Nakajima, Advances in bone joint imaging-metal artifact reduction, *Diagnostics* 12 (2022) 3079, <https://doi.org/10.3390/diagnostics12123079>.
- [52] H. Xie, L. Xie, J. Wang, C. Chen, C. Zhang, W. Zheng, Intramedullary versus extramedullary fixation for the treatment of subtrochanteric fracture: a systematic review and meta-analysis, *Int. J. Surg.* 63 (2019) 43–57, <https://doi.org/10.1016/j.ijsu.2019.01.021>.
- [53] W. Sheng, A. Ji, R. Fang, G. He, C. Chen, Finite element-and design of experiment-derived optimization of screw configurations and a locking plate for internal fixation system, in: *Computational and Mathematical Methods in Medicine 2019*, 2019.
- [54] R. Fang, A. Ji, Z. Zhao, D. Long, C. Chen, A regression orthogonal biomechanical analysis of internal fixation for femoral shaft fracture, *Biocybern. Biomed. Eng.* 40 (2020) 1277–1290, <https://doi.org/10.1016/j.bbe.2020.07.006>.